PCCP

PAPER

View Article Online
View Journal | View Issue

Cite this: *Phys. Chem. Chem. Phys.*, 2021, **23**, 10267

Needles in a haystack: H-bonding in an optogenetic protein observed with isotope labeling and 2D-IR spectroscopy†

Jeannette Ruf, Peter Hamm and David Buhrke *

Received 5th March 2021,
Accepted 9th April 2021

DOI: 10.1039/d1cp00996f

rsc.li/pccp

Recently, re-purposing of cyanobacterial photoreceptors as optogentic actuators enabled light-regulated protein expression in different host systems. These new bi-stable optogenetic tools enable interesting new applications, but their light-driven working mechanism remains largely elusive on a molecular level. Here, we study the optogenetic cyanobacteriochrome Am1-c0023g2 with isotope labeling and two dimensional infrared (2D-IR) spectroscopy. Isotope labeling allows us to isolate two site-specific carbonyl marker modes from the overwhelming mid-IR signal of the peptide backbone vibrations. Unlike conventional difference-FTIR spectroscopy, 2D-IR is sensitive to homogeneous and inhomogeneous broadening mechanisms of these two vibrational probes in the different photostates of the protein. We analyse the 2D-IR line shapes in the context of available structural models and find that they reflect the hydrogen-bonding environment of these two marker groups.

I. Introduction

Cyanobacteriochromes (CBCRs) are photosensitive proteins that regulate diverse cellular responses to environmental light conditions in cyanobacteria.[1–3] This class of proteins recently recieved increasing attention as building blocks for optogenetic tools because their modular domain structure allows to light-trigger cellular responses in different target organisms.[4–7] One example is the light-regulated expression of target genes, which was recently achieved in yeast with a two-component optogenetic system[8] based on the red/green CBCR Am1-c0023g2 (from here abbreviated AmI-g2) from the cyanobacterium *Acarychloris marina*.[9] AmI-g2 is a member of the red/green lineage of CBCRs and can incorporate two different light-sensitive chromophores: phycocyanobilin (PCB) or biliverdin. Here, we investigate the PCB-assembled protein variant (Fig. 1) which can reversibly switch between a red- and green-light absorbing state (Pr and Pg, respectively).

All CBCRs share a common protein fold (called GAF fold) shown in Fig. 1A. They autocatalytically form a covalent thioether bond to the chromophore *via* addition of a conserved cysteine residue to tetrapyrrole ring A (Fig. 1B). Despite the fact that different CBCRs have been studied extensively with crystallographic,[10–12] biochemical and spectroscopic methods, there is an ongoing debate about the role of structural heterogeneity. There are many evidences for the presence of several conformational sub-states with distinct properties in red/green CBCRs from nuclear magnetic resonance (NMR),[13,14] resonance Raman[15,16] or ultrafast optical spectroscopy.[17–20] In these ultrafast spectroscopic studies, ground state structural heterogenieties were inferred from two observations in the past: (1) excitation wavelength dependence and (2) multiphasic behaviour of the excited state decay kinetics. While (2) can also be explained by solvation processes,[21,22] the many other observations leave open questions: what exactly is heterogeneous in CBCRs and on which timescales does it equilibrate? Are the heterogenieties relevant for the function of CBCRs? There is some progress, especially from NMR and theoretical studies that ascribe these observations for example mixed conformations of tryptophan residues[13–15] or the protonation of histidine residues.[23] However NMR has intrinisically slow time resolution, and there are up to now no experimental studies that access the ultrafast dynamics of the electronic ground states. Here, we employ two dimensional infrared (2D-IR) spectroscopy in combination with isotope editing to isolate two vibrational modes that provide site-specific information about their direct environment within the protein in the Pr and Pg states. 2D-IR is a powerful tool to monitor the ultrafast dynamics of these modes and detect heterogenieties and their spectral diffusion with picosecond time-resolution.[24] We observe various degrees of homogenous and inhomogenous broadening in the 2D-IR signals and relate them to differences in hydrogen-bonding.

Department of Chemistry, University of Zürich, Zürich, Switzerland.
E-mail: david.buhrke@chem.uzh.ch

† Electronic supplementary information (ESI) available. See DOI: 10.1039/d1cp00996f

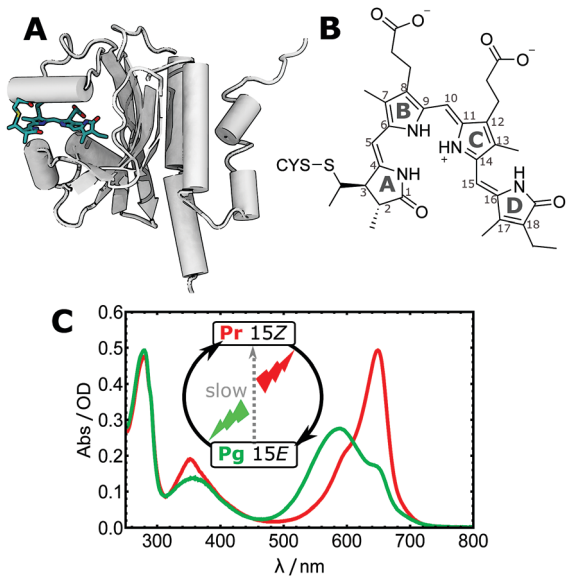

Fig. 1 Molecular properties of the red/green CBCR AmI-g2. (A) the protein adopts the typical GAF fold and covalently binds a PCB chromophore (cyan) to a conserved cysteine residue. Shown here is the crystal structure of the homologous GAF2 domain from the CBCR AnPixJ (PDB entry 3W2Z). (B) Structure of the PCB chromophore in the Pr state with the C15═C16 double bond in *Z* configuration. (C) UV-vis absorption spectra of the Pr and Pg states.

II. Materials and methods

Protein expression and purification

The apo AmI-g2 expressing cells were generated by transforming *E. coli* BL21 with a pET-30a(+) vector (kanamycin resistance) containing the sequence for AmI-g2 apo in the open reading frame (GenScript Biotech, Piscataway Township NJ, USA). The translated apo AmI-g2 includes a C-terminal His6-tag which was used to purify the protein under native conditions *via* Ni-affinity chromatography. Cells were grown at 37 °C and 155 rpm in Luria broth (LB) medium containing 35 μg ml^{-1} kanamycin to an OD_{600} of 0.6–0.8. M9 minimal medium containing ^{13}C-glucose and ^{15}N-ammoniumchloride was used for the expression of globally $^{13}C^{15}N$-labeled protein. All cultures were induced with 1 mM isopropyl β-D-1-thiogalactopyranoside (IPTG). After incubation overnight at room temperature and 155 rpm, cells were harvested by centrifugation and stored at −20 °C. A shorter incubation time of 4 h was used for the isotope edited protein variant. The apo-protein was purified under native conditions *via* Ni-affinity chromatography and desalted into a reducing buffer based on PBS that also contained 5 mM EDTA and 5 mM β-mercaptoethanol using a Sephadex HiPrep 26/10 column (GE Healthcare Bio-Sciences, Uppsala, Sweden). 25 mM PCB in DMSO was added in 1.5× molar excess to the apoprotein and the *in vitro* assembly of AmI-g2-PCB was monitored using UV-vis spectroscopy. After *ca.* 30 min, no spectral changes were observed and the reaction mixture was desalted again into the final PBS buffer, thereby removing unbound PCB, EDTA and β-mercaptoethanol. For all IR experiments, the samples were prepared in D_2O buffer by lyophilization as described earlier[25] and deposited in CaF_2 sandwich cells with 25 μm path length.

2D-IR spectroscopy

2D-IR experiments were performed with a previously described setup.[26] Briefly, the output of a Yb-doped fiber laser/amplifier system (short-pulse Tangerine, Amplitude, France) with a repetition rate of 100 kHz was converted to the mid-IR with an OPA (Twin STARZZ, Fastlite, France) and subsequent frequency mixing. The IR pulses were split into pump, probe and reference pulses, and the pump pulses were sent through a pulse shaper (PhaseTech Spectroscopy) to generate a pulse pair with programmable delay times and phases. Working in a rotating frame, the delays were scanned in 50 fs time steps (spectral resolution of pump axis is 8 cm^{-1}) and 4 phase cycles were used to suppress scattering. The delay between the pump pulse pair an the probe pulse (t_2) was controlled with a conventional delay stage. Pump and probe pulses were focused and overlapped in the sample (spot size 100 μm), while the reference was slightly offset (*ca.* 500 μm). Probe and reference beams were transmitted through a spectrograph and detected with a 2 × 32-MCT detector array (spectral resolution *ca.* 4 cm^{-1}) with custom electronics.[27] The samples were prepared either in the Pr state by illumination with a green LED array (LIU525B, Thorlabs, Newton, MA, USA) or kept in the Pg state by illumination a red laser diode (HL6750MG) during the measurements. This illumination procedure resulted in a photostationary equilibrium with less than 20% residual Pr contribution in the Pg samples (see ESI†).

III. Results

Labeling and FTIR

IR spectra of photoreceptor proteins in the region between 1600 and 1750 cm^{-1} contain overlapping contributions from different vibrational modes. Like in all other proteins, this region is dominated by the amide I vibrations from the protein backbone (termed I′ in deuterated samples), but also contains C═O stretching vibrations from amino acid side chains[28] and vibrational modes from the light-sensitive co-factor.[16] These contributions can be distinguished from each other by isotope labeling parts of the system and comparing the IR spectra. Here, we $^{13}C^{15}N$-labeled the entire AmI-g2 apo-protein and incooperated isotope-normal PCB. Fig. 2A shows Fourier transform IR (FTIR) absorption spectra of the labeled and normal samples with emphasis on the downshift of the amide I′ mode by *ca.* 50 cm^{-1} upon labeling (blue line). FTIR spectra of labeled and isotope normal AmI-g2 samples were recorded in the Pr and Pg states, and the corresponding "Pg-minus-Pr" difference spectra are shown in Fig. 2B. Some of the light-induced difference bands display the same shift pattern (downshifts by *ca.* 50 cm^{-1}), and we can assign these to amide I′ difference bands that originate from structural changes of the protein backbone between the Pr and Pg states (indicated by red arrows). On the other hand, two difference-bands in the region between 1650 and 1760 cm^{-1} are completely insensitive to isotope labeling of the protein, and thus must

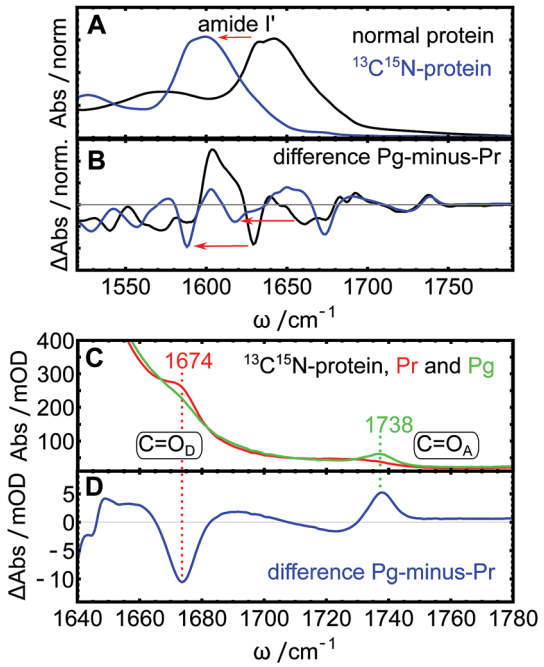

Fig. 2 FTIR spectra of isotope-normal and $^{13}C^{15}N$-labeled AmI-g2. (A) Downshift of the amide I′ mode (red arrows) in the labeled protein (blue line) compared to the isotope normal protein (black line). (B) Pg-minus-Pr difference spectra of the two variants. (C) Detailed view of the C=O stretching region of the $^{13}C^{15}N$ protein in the Pr state (red line) and Pg state (green line), frequencies of the two C=O bands indicated. (D) Detailed view of the difference spectrum in the same region.

originate from PCB. In the labeled sample, the collective tails of the downshifted amide I′ modes contribute to this spectral region only in the form of background absorption, and therefore both PCB bands are clearly visible in the absolute and the difference spectra (Fig. 2C and D). We assign these two bands to the carbonyl stretching vibrations of the pyrrole rings D (C=O$_D$ at 1674 cm^{-1}) and A (C=O$_A$ at 1738 cm^{-1}) based on the literature.[29–31] Here, isotope labeling of individual carbon or oxygen atoms in PCB showed that the two carbonyl bands appear consistently at these position in several PCB-binding photoreceptors and model compounds. In PCB, pyrrole ring A is saturated, while all atoms in ring D are part of the conjugated system (see Fig. 1B), which accounts for major portion of the *ca.* 60 cm^{-1} frequency difference between the respective bands.[29,30] Both bands show drastic changes in line shape depending on illumination. While C=O$_A$ is very broad and hardly distinguishable from the background in Pr, it shows up as a clear narrow peak at 1738 cm^{-1} in Pg. Interestingly, C=O$_D$ behaves opposite: it is quite narrow and well defined in Pr state at 1674 cm^{-1}, and broadens in Pg. This observation also becomes very evident from the difference spectra (Fig. 2D), and reflects how the carbonyl groups sense their different environment in the Pr and Pg states. We now turn to 2D-IR spectroscopy to investigate these two bands in more depth.

2D-IR spectroscopy

2D-IR spectra in the region between 1640 and 1780 cm^{-1} were recorded for AmI-g2 in the Pr and Pg states at different population times t_2 from 200 fs up to 3 ps (Fig. 3 shows the isotope labeled sample, isotope normal in ESI†). 2D-IR intensities scale with the square of the absorption cross section, while the linear absorbance scales linearly with the cross section.[24] Therefore, the amide I′ background appears further suppressed in the 2D-IR spectra despite its high linear absorbance (compare to Fig. 2C). In the isotope labeled sample, both target C=O bands can now be clearly detected in both states, and we do not observe any cross-peaks. In 2D-IR spectra, each signal consists of a negative peak on the diagonal axis (blue, ground state bleach and stimulated emission) and a positive counterpart (red, excited state absorption) shifted along the probe axis ω_{probe} due to anharmonicity.[24] All 2D signals decay with increasing t_2 due to vibrational population relaxation, and spectra collected at short t_2 delays (*e.g.* 200 fs) have a higher signal-to-noise ratio than at long t_2 delays. In Fig. 3, this decay was normalized out in the right panels, and spectra taken at 2 ps therefore appear more noisy. The vibrational lifetimes of the two modes in both states are around 1 ps, which is a typical value for carbonlys that usually decay between 0.8 and 5 ps.[32]

The first important observable from 2D-IR spectroscopy is the 2D line shape, which allows to distinguish between homogeneous and inhomogeneous broadening mechanisms. A homogeneous band appears round, while an inhomogeneously broadened band that arises from many different sub-states with slightly different frequencies appears elongated along the diagonal.[24] The two narrow bands that were identified in the FTIR spectra (C=O$_D$ in Pr C=O$_A$ in Pg) appear homogeneously broadened in the 2D-IR spectra, while the broad bands (C=O$_D$ in Pg and C=O$_A$ in Pr) are clearly inhomogeneously broadenend. The second important observable in 2D-IR is the t_2-evolution of the center line slope (CLS), called spectral diffusion, which is a direct measure of equilibration on a ps time scale (CLS are indicated coloured bars in Fig. 3). While a perfectly homogeneous band has a horizontal center line (CLS = 0), heterogeneous broadening leads to tilted center lines as the peaks are elongated along the diagonal (45° or CLS = 1). A decrease of the CLS with increasing t_2 indicates an equilibration of the sub-states on this time scale.[24] We observe a kink in the CLS of C=O$_A$ in the Pr state, indicating that this band consists of at least two distinguishable contributions with different CLS (red and magenta). This behaviour is highlighted in the diagonal cuts in Fig. 4. For C=O$_A$(Pr), we observe a main peak at the same frequency as Pg (1736 cm^{-1}), and a shoulder at 1720 cm^{-1}. We attribute this shoulder to an additional sub-state of C=O$_A$ in the Pr state. We therefore treat C=O$_A$(Pr) as two different bands centered at 1720 (magenta) and 1736 cm^{-1} (red). In line with the previous analysis, the homogeneous bands (C=O$_D$(Pr) and C=O$_A$(Pg)) already have lower CLS (*ca.* 0.4) compared to the broad C=O$_D$(Pg) (*ca.* 0.8) after 200 fs. The low CLS of the narrow peaks decreases further with t_2 (Fig. 4, bottom panels), which indicates that a comparably small heterogeneous component arises from fast fluctuations on the ps time scale. In contrast, the CLS of the the broad C=O$_D$(Pg) band does not decay in the investigated time-window, indicating that the heterogeneous broadening arises from sub-states which equilibrate only on

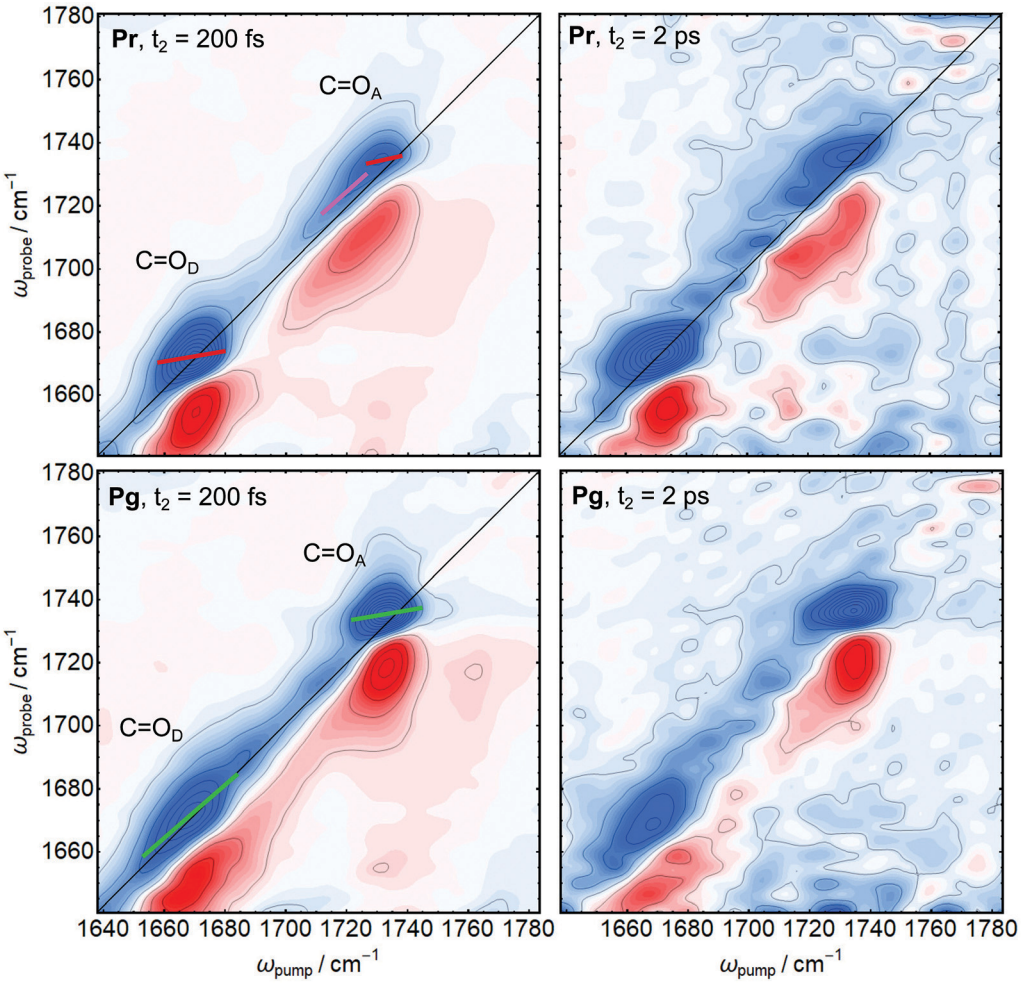

Fig. 3 2D-IR spectra of AmI-g2 in the Pr (top row) and Pg states (bottom row) at different population times. Spectra taken at t_2 = 200 fs are shown on the left side, t_2 = 2 ps on the right side. CLS of different bands are indicated as red, magenta and green lines.

longer time scales that are not accessible due to the fast vibrational relaxation of all bands. Here, meaningful values for the CLS can only be obtained up to 2.5 ps due to the increasing noise level. The 1720 cm^{-1} component of C=O$_A$(Pr) has a CLS of 0.7, while the 1736 cm^{-1} component is more homogeneous with a CLS of 0.4 and both do not decay in the accessible time window.

IV. Discussion

Spectral tuning of carbonyl frequencies

Three different factors are known to have major influence the frequency of C=O vibrations: the chemical structure of the investigated compound, hydrogen bonding and electric fields.[33] As already mentioned beforehand, the chemical structure (saturation of PCB) is the main reason why the two carbonyl stretches are detected at different frequencies. Furthermore, carbonyls are known to be very sensitive to hydrogen bond donation, where each oxygen can accept up to two H-bonds, and experience red shifts by *ca.* 15–25 cm^{-1} with each additional H-bond.[33,34] In AmI-g2, we observe only neglible shifts of the peak positions for both investigated carbonyl groups upon photoconversion (Fig. 4), but predominately changes in line shapes. The line shapes are either homogeneous, narrow and symmetric around their maximum frequencies or show strong heterogeneous broadening, which we attribute to heterogeneous H-bonding environments sensed by the carbonyl groups.

Ring D carbonyl

There are three molecular structures available for red/green CBCRs in the Pr state that show strong similarities, namely AnPixJg2,[11] NpR6012g4[13] and Slr1393g3.[12] In all these structures, the ring D carbonyl is buried entirely inside the protein in H-bond distance with one conserved tyrosin residue. This conserved position is reflected in the 2D-IR spectra by the homogeneous band with a fast decaying, low CLS. While the different CBCRs of the red/green lineage have highly similar structures and spectral properties in the Pr state, their Pg states are much more diverse. Common to all, PCB is isomerised around the C15=C16 bond, which leads to a rotation of ring D and consequently an entirely different protein environment compared to the Pr state. In the Pg structures of NpR6012g4[13] and Slr1393g3,[12] C=O$_D$ moves into a solvent accessible position,

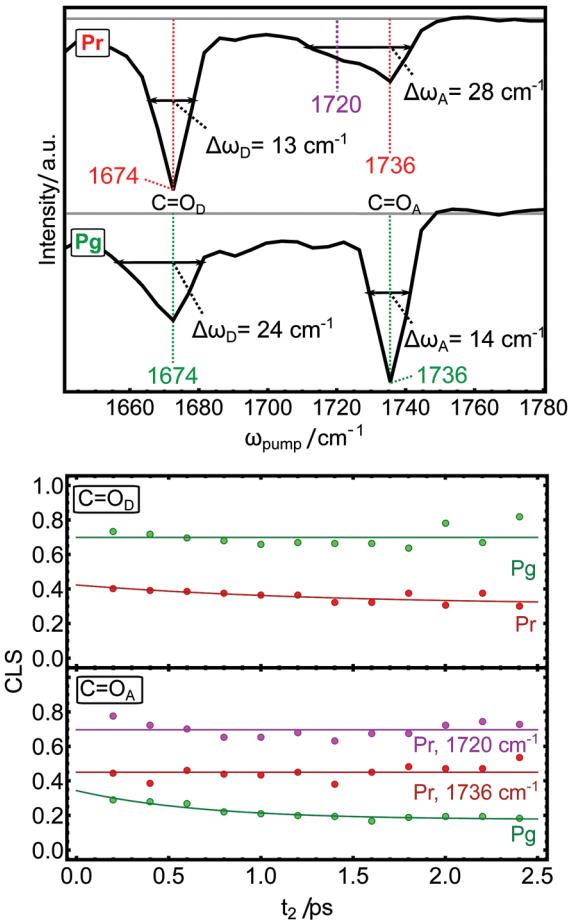

Fig. 4 Top panels: Diagonal cuts of the 2D-IR spectra in the Pr and Pg states. Bottom panels: The t_2-evolution of the CLS of the carbonyl modes in the Pg state (green traces) and Pr state (red and magenta traces).

which is occupied by a sodium ion in case of Slr1393g3. We observe a heterogeneous broadening of C=O$_D$ band with shoulders on both sides in Pg, while the center frequency does not shift. This is in line with a solvent accessible position in the Pg state, where the carbonyl can interact with zero to two interaction partners, *i.e.* water, ions, or other residues. On average, these interactions have the same effect on the carbonyl as the single H-bond to the Tyr residue in Pr, which accounts for the same central peak position. In the difference-FTIR spectra, this broadening in a heterogeneous environment is reflected by a sharp negative contribution at 1674 cm^{-1} on top of a broad positive background, which was also observed at similar frequencies in the difference FTIR spectra of AnpixJg2,[35,36] NpR6012g4[37] and Slr1393g3.[25]

Ring A carbonyl

In contrast to the C=O$_D$, the ring A carbonyl is H-bonded to a conserved tryptophan residue in the crystal structures of AnPixJg2 and Slr1393g3, but a heterogeneity is found in the NMR structure of NpR6012g4. Here, a two-state behaviour is observed, where the H-bond is sometimes broken and the tryptophan moves away from ring A. These two states were also

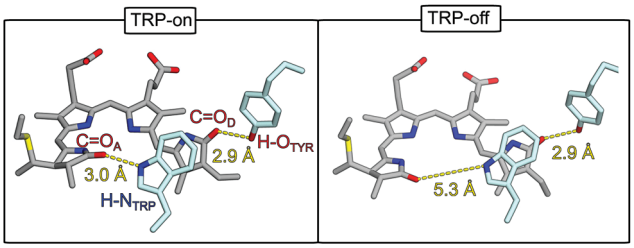

Fig. 5 Tryptophan heterogeneity in the Pr state of the red/green CBCR AnPixJg2 observed by MD simulations.[23] This figure was kindly provided by A. Rao and I. Schapiro.

observed in molecular dynamics simulations of AnPixJg2 independently by two different research groups, and the results of Rao *et al.* are shown in Fig. 5.[14,23] Resonance Raman spectra of Slr1393g3 in the Pr state could be decomposed into the two sub-states, confirming the two-state nature for a third member of the red/green lineage and providing insight into the differences of PCB configuration and fluorescence properties of the two states.[16] These two sub-states are observed in the 2D-IR spectra at 1720 (H-bond) and 1736 cm^{-1} (no H-bond). Interestingly, the H-bonded shoulder is heterogeneously broadened and maintains a high CLS of *ca.* 0.7 over the accessible time range, which reflects different H-bond strengths or distances between Trp and the ring A carbonyl. These states do not equilibrate on a ps timescale because they involve movements of the protein which expected to be much slower, but the transition can be observed on a ns time scale in the computer simulations. On the other hand, the higher frequency band is homogeneous with a constant CLS of 0.4, which agrees well with the assignment to the non H-bonded state. Interestingly, the indole group of the Trp residue forms a pi-stacking interaction with PCB ring D only in the Trp-on state, which apparently has negligible impact on the homogenous appearing C=O$_D$. This result is in good agreement with a previous resonance Raman study of the related CBCR Slr-g3, where it was shown that the Trp sub-states are not sensed by other vibrational modes associated with ring D, but strongly by ring A.[16] The published FTIR spectra of other red/green CBCRs differ quite substantially for C=O$_A$, where the other proteins only show a weak bleach band in the FTIR difference spectra,[25,35–37] and only AmI-g2 displays the sharp positive feature. In line with the assignment of the two C=O$_A$ bands in the Pr state, we conclude that in the Pg state of AmI-g2, the C=O$_A$ must be located in a hydrophobic environment that does not allow H-bonding. This transition apparently does not take place in other red/green CBCRs.

V. Conclusions

While spectroscopic studies consistently showed that heterogeneity plays an important role in many CBCRs, the molecular basis for these observation is often unclear, mainly because most studies employ methods lacking spatial resolution (like transient vis spectroscopy). In this study, we gain site-specific information through isotope labeling and employ 2D-IR spectroscopy based

on a novel 100 kHz Yb laser system, which provides a sufficient signal-to-noise ratio to detect only two localized carbonyl modes in a protein composed of 166 amino acids within a reasonable acquisition time. Remarkably, we find that the peak positions of both carbonyl marker modes do not shift upon photoconversions but instead change line shape. Shifts or broadenings cannot be distinguished by difference-FTIR spectroscopy, and we speculate that broadening might also be the main reason for C=O difference signals in other bilin-photoreceptors, which are frequently interpreted in terms of frequency shifts. We observe that some modes are homogeneously broadened and quickly equilibrate to a large extent on a ps time scale, while others are inhomogenously broadened and do not equilibrate in the accessible time window. Analysis of our observations in the context of the available structural models for red/green CBCRs shows that spectral broadening correlates with heterogeneity in the hydrogen-bonding environment. Here, the $C{=}O_A$ vibration in the Pr state is an extreme case, where a two-state (H bond on/off) behaviour is reflected by two different carbonyl stretching frequencies with distinctive 2D line shapes.

Author contributions

DB and JR expressed and purified the protein. JR and DB performed spectroscopic experiments. DB, JR and PH analysed the data. DB wrote the MS with contributions of all authors.

Data availability statement

The data are openly available on Zenodo at 10.5281/zenodo.4650475.

Conflicts of interest

There are no conflicts of interest to declare.

Acknowledgements

The authors would like to thank A. Rao and I. Schapiro for providing their results and Fig. 5 prior to publication. We thank Jan Helbing and Roland Zehnder for technical support and Ricardo Fernández-Terán for help with the CLS analysis. This work was supported by the Swiss National Science Foundation (SNF) through the NCCR MUST and Grant 200020B_188694/1.

References

1 K. Anders and L. O. Essen, *Curr. Opin. Struct. Biol.*, 2015, **35**, 7–16.
2 K. Fushimi and R. Narikawa, *Curr. Opin. Struct. Biol.*, 2019, **57**, 39–46.
3 N. C. Rockwell and J. C. Lagarias, *Curr. Opin. Plant Biol.*, 2017, **37**, 87–93.
4 M. Blain-Hartung, N. C. Rockwell, M. V. Moreno, S. S. Martin, F. Gan, D. A. Bryant and J. C. Lagarias, *J. Biol. Chem.*, 2018, **293**, 8473–8483.
5 N. T. Ong and J. J. Tabor, *ChemBioChem*, 2018, **19**, 1255–1258.
6 Z. Liu, J. Zhang, J. Jin, Z. Geng, Q. Qi and Q. Liang, *Front. Microbiol.*, 2018, **9**, 1–11.
7 S. M. Castillo-Hair, E. A. Baerman, M. Fujita, O. A. Igoshin and J. J. Tabor, *Nat. Commun.*, 2019, **10**, 1–11.
8 J. Jang, S. McDonald, M. Uppalapati and A. Woolley, *bioRxiv, Synth. Biol.*, 2019, 1–23.
9 K. Fushimi, T. Nakajima, Y. Aono, T. Yamamoto, Ni-Ni. Win, M. Ikeuchi, M. Sato and R. Narikawa, *Front. Microbiol.*, 2016, **7**, 1–12.
10 E. S. Burgie, J. M. Walker, G. N. Phillips and R. D. Vierstra, *Structure*, 2013, **21**, 88–97.
11 R. Narikawa, T. Ishizuka, N. Muraki, T. Shiba, G. Kurisu and M. Ikeuchi, *Proc. Natl. Acad. Sci. U. S. A.*, 2013, **110**, 918–923.
12 X. Xu, A. Port, C. Wiebeler, K. H. Zhao, I. Schapiro and W. Gärtner, *Proc. Natl. Acad. Sci. U. S. A.*, 2020, **117**, 2432–2440.
13 S. Lim, Q. Yu, S. M. Gottlieb, C.-W. Chang, N. C. Rockwell, S. S. Martin, D. Madsen, J. C. Lagarias, D. S. Larsen and J. B. Ames, *Proc. Natl. Acad. Sci. U. S. A.*, 2018, **115**, 4387–4392.
14 L. K. Scarbath-Evers, S. Jähnigen, H. Elgabarty, C. Song, R. Narikawa, J. Matysik and D. Sebastiani, *Phys. Chem. Chem. Phys.*, 2017, **19**, 13882–13894.
15 F. Velázquez Escobar, T. Utesch, R. Narikawa, M. Ikeuchi, M.-A. Mroginski, W. Gärtner and P. Hildebrandt, *Biochemistry*, 2013, **52**, 4871–4880.
16 D. Buhrke, G. Battocchio, S. Wilkening, M. Blain-Hartung, T. Baumann, F. J. Schmitt, T. Friedrich, M. A. Mroginski and P. Hildebrandt, *Biochemistry*, 2020, **59**, 509–519.
17 P. W. Kim, L. H. Freer, N. C. Rockwell, S. S. Martin, J. C. Lagarias and D. S. Larsen, *Biochemistry*, 2012, **51**, 608–618.
18 S. M. Gottlieb, P. W. Kim, C. W. Chang, S. J. Hanke, R. J. Hayer, N. C. Rockwell, S. S. Martin, J. C. Lagarias and D. S. Larsen, *Biochemistry*, 2015, **54**, 1028–1042.
19 J. S. Kirpich, S. M. Gottlieb, C. W. Chang, P. W. Kim, S. S. Martin, J. C. Lagarias and D. S. Larsen, *Biochemistry*, 2019, **58**, 2307–2317.
20 C. Slavov, X. Xu, K. H. Zhao, W. Gärtner and J. Wachtveitl, *Biochim. Biophys. Acta, Bioenerg.*, 2015, **1847**, 1335–1344.
21 D. Wang, X. Li, S. Zhang, L. Wang, X. Yang and D. Zhong, *Proc. Natl. Acad. Sci. U. S. A.*, 2020, **117**, 19731–19736.
22 D. Wang, X. Li, L. Wang, X. Yang and D. Zhong, *J. Phys. Chem. Lett.*, 2020, **11**, 8819–8824.
23 A. G. Rao, C. Wiebeler, S. Sen, D. S. Cerutti and I. Schapiro, *Phys. Chem. Chem. Phys.*, 2021, 7–13.
24 P. Hamm and M. T. Zanni, *Concepts and Methods of 2D Infared Spectroscopy*, Cambridge University Press, 2011.
25 D. Buhrke, K. T. Oppelt, P. J. Heckmeier, R. Fernández-Terán and P. Hamm, *J. Chem. Phys.*, 2020, **153**, 245101.
26 P. Hamm, *J. Chem. Phys.*, 2021, **154**, 1–6.
27 K. M. Farrell, J. S. Ostrander, A. C. Jones, B. R. Yakami, S. S. Dicke, C. T. Middleton, P. Hamm and M. T. Zanni, *Opt. Express*, 2020, **28**, 33584–33602.
28 A. Barth and C. Zscherp, *Q. Rev. Biophys.*, 2002, **35**, 369–429.
29 F. Siebert, R. Grimm, W. Rüdiger, G. Schmidt and H. Scheer, *Eur. J. Biochem.*, 1990, **194**, 921–928.

30 H. Foerstendorf, C. Benda, W. Gärtner, M. Storf, H. Scheer and F. Siebert, *Biochemistry*, 2001, **40**, 14952–14959.
31 J. J. van Thor, N. Fisher and P. R. Rich, *J. Phys. Chem. B*, 2005, **109**, 20597–20604.
32 S. H. Schneider, H. T. Kratochvil, M. T. Zanni and S. G. Boxer, *J. Phys. Chem. B*, 2017, **121**, 2331–2338.
33 V. A. Lorenz-Fonfria, *Chem. Rev.*, 2020, **120**, 3466–3576.
34 S. Woutersen, Y. Mu, G. Stock and P. Hamm, *Chem. Phys.*, 2001, **266**, 137–147.
35 Y. Fukushima, M. Iwaki, R. Narikawa, M. Ikeuchi, Y. Tomita and S. Itoh, *Biochemistry*, 2011, **50**, 6328–6339.
36 C. Song, F. Velázquez Escobar, X. L. Xu, R. Narikawa, M. Ikeuchi, F. Siebert, W. Gärtner, J. Matysik and P. Hildebrandt, *Biochemistry*, 2015, **54**, 5839–5848.
37 J. S. Kirpich, C. W. Chang, J. Franse, Q. Yu, F. V. Escobar, A. J. Jenkins, S. S. Martin, R. Narikawa, J. B. Ames, J. C. Lagarias and D. S. Larsen, *Biochemistry*, 2021, **60**, 274–288.